Inorganic Chemistry

ARTICLE

pubs.acs.org/IC

Study of the Luminescent and Magnetic Properties of a Series of Heterodinuclear [$Zn^{II}Ln^{III}$] Complexes

Traian D. Pasatoiu,[†] Carmen Tiseanu,[*,‡] Augustin M. Madalan,[†] Bogdan Jurca,[§] Carine Duhayon,[∥,⊥] Jean Pascal Sutter,[*,∥,⊥] and Marius Andruh[*,†]

[†]University of Bucharest, Faculty of Chemistry, Inorganic Chemistry Laboratory, Str. Dumbrava Rosie nr. 23, 020464-Bucharest, Romania

[‡]National Institute for Laser, Plasma and Radiation Physics, Laboratory of Solid-State Quantum Electronics, P.O. Box MG-36, Magurele, 077125, Romania

[§]University of Bucharest, Faculty of Chemistry, Department of Physical Chemistry, Bd. Regina Elisabeta nr. 4-12, Bucharest, Romania

[∥]CNRS, LCC (Laboratoire de Chimie de Coordination), 205, route de Narbonne, F-31077 Toulouse, France

[⊥]Université de Toulouse, UPS, INPT, LCC, F-31077 Toulouse, France

Supporting Information

ABSTRACT: Herein, we report the synthesis, structural investigation, and magnetic and photophysical properties of a series of 13 [$Zn^{II}Ln^{III}$] heterodinuclear complexes, which have been obtained employing a Schiff-base compartmental ligand derived from *o*-vanillin [H_2valpn = 1,3-propanediylbis(2-iminomethylene-6-methoxy-phenol)]. The complexes have been synthesized starting from the [Zn(valpn)(H_2O)] mononuclear compound and the corresponding lanthanide nitrates. The crystallographic investigation indicated two structural types: the first one, [Zn(H_2O)(valpn)Ln^{III}(O_2NO)$_3$], contains 10-coordinated Ln^{III} ions, while in the second one, [Zn(ONO_2)(valpn)-Ln^{III}(H_2O)(O_2NO)$_2$]·2H_2O, the rare earth ions are nine-coordinated. The Zn^{II} ions always display a square-pyramidal geometry. The first structural type encompasses the larger Ln ions ($4f^0$−$4f^9$), while the second is found for the smaller ions ($4f^8$−$4f^{11}$). The dysprosium derivative crystallizes in both forms. Luminescence studies for the heterodinuclear compounds containing Nd^{III}, Sm^{III}, Tb^{III}, Dy^{III}, and Yb^{III} revealed that the [Zn(valpn)(H_2O)] moiety acts as an antenna. The magnetic properties for the paramagnetic [$Zn^{II}Ln^{III}$] complexes have been investigated.

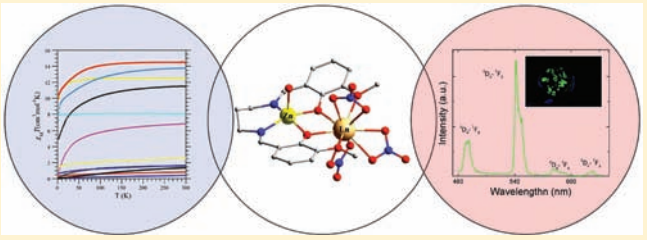

INTRODUCTION

Numerous studies of the lanthanide complexes arise from their unique luminescence properties, which make them appropriate for a wide range of applications such as luminescent probes in analytical time-resolved fluoroimmunoassays, imaging and sensor applications where time-gating techniques can be applied to eliminate competitive autofluorescent signals (short nanosecond fluorescence) from surrounding biological molecules,[1] novel materials, and probes in biomedical applications and optical technologies (light-emitting diodes, laser systems, dopants in electroluminescent devices, and optical amplification for telecommunications).[2]

The luminescence applications of lanthanides are a consequence of their narrow emission bands, with negligible environmental influences since the 4f electrons are shielded by filled 5s and 5p orbitals, a large Stokes' shift, and relatively long luminescence lifetimes (ranging from nanosecond to millisecond order) as a result of transitions within the partially filled 4f shell of the ions.[3]

Because the f−f transitions are parity forbidden, as the effective relaxation of the Laporte selection rule is generally disfavored,[4] the absorption coefficients are normally very low, and the emissive rates are slow. This disadvantage may be overcome by using well-designed organic chromophores which act as sensitizers to excite lanthanide ions (antenna effect).[4,5]

On the other hand, the large and anisotropic magnetic moment for some of the Ln^{III} ions makes them very appealing for the preparation of magnetic materials. All of the paramagnetic Ln^{III} ions, except Gd^{III}, have degenerate ground states that are split by spin−orbit coupling and crystal-field effects, which makes their orbital component of the magnetic moment much more important than for the transition-metal ions.[6] It is known that hexadentate Schiff-bases derived from *o*-vanillin and diamines can lead to heterodinuclear 3d−4f complexes because they have two differentiated sites: an inner site with N- and O-donor chelating centers which can accommodate 3d ions (radii 0.75−0.6 Å) and a larger outer coordination site with four O-donor atoms which is able to incorporate large ions, such as the oxophilic lanthanide ions (radii 1.06−0.85 Å). Most of the studies of the heterodinuclear 3d−4f complexes with acyclic hexadentate Schiff bases have been focused

Received: March 2, 2011
Published: June 02, 2011

Table 1. Crystal Data and Refinement for the Types I and II Heterodinuclear Compounds 1−12

compound	1	3	5	6	7	8	9
chemical formula	$C_{19}H_{22}N_5O_{14}ZnLa$	$C_{19}H_{22}N_5O_{14}ZnPr$	$C_{19}H_{22}N_5O_{14}ZnSm$	$C_{19}H_{22}N_5O_{14}ZnEu$	$C_{19}H_{22}N_5O_{14}ZnGd$	$C_{19}H_{22}N_5O_{14}ZnTb$	$C_{19}H_{22}N_5O_{14}ZnDy$
M (g mol^{-1})	748.68	749.89	760.14	761.76	767.05	768.69	772.29
temp (K)	293(2)	180	293(2)	293(2)	293(2)	293(2)	180
wavelength (Å)	0.71073	0.71073	0.71073	0.71073	0.71073	0.71073	0.71073
cryst syst	monoclinic	monoclinic	monoclinic	monoclinic	monoclinic	monoclinic	monoclinic
space group	$P2_1/c$	$P2_1/c$	$P2_1/c$	$P2_1/c$	$P2_1/c$	$P2_1/c$	$P2_1/c$
a (Å)	9.0232(6)	8.8636(3)	8.9838(3)	8.9419(4)	8.9343(3)	8.9308(4)	8.8412(2)
b (Å)	29.027(3)	28.9754(7)	29.4974(13)	29.2149(13)	29.2116(13)	29.2003(9)	29.0027(10)
c (Å)	10.2900(6)	10.1774(4)	10.1127(4)	10.1778(4)	10.1603(3)	10.1584(5)	10.0702(3)
α (deg)	90.00	90.00	90.00	90.00	90.00	90.00	90.00
β (deg)	103.015(5)	102.853(4)	103.122(3)	103.496(3)	103.538(3)	103.682(3)	103.294(3)
γ (deg)	90.00	90.00	90.00	90.00	90.00	90.00	90.00
V (Å^3)	2625.8(4)	2548.33(15)	2609.88(18)	2585.40(19)	2578.01(16)	2573.95(19)	2512.99(13)
Z	4	4	4	4	4	4	4
D_c (g cm^{-3})	1.889	1.954	1.929	1.952	1.971	1.978	2.041
μ (mm^{-1})	2.596	2.911	3.225	3.411	3.560	3.737	3.987
F(000)	1472	1488	1492	1496	1500	1504	1516
refinement on	F^2	F	F^2	F^2	F^2	F^2	F
goodness of fit	1.030	1.1612	1.042	1.075	1.166	1.048	1.0854
final R_1, wR_2	0.0661, 0.1344	0.0243, 0.0213	0.0557, 0.1373	0.0544, 0.1151	0.0728, 0.1345	0.0524, 0.1064	0.0177, 0.0211
$[I > n\sigma(I)]$	$n = 2$	$n = 3$	$n = 2$	$n = 2$	$n = 2$	$n = 2$	$n = 3$
R_1, wR_2 (all data)	0.1180, 0.1523	0.0322, 0.0220	0.0701, 0.1447	0.0794, 0.1258	0.0864, 0.1402	0.0722, 0.1132	0.0334, 0.0249
largest diff. peak and hole (e Å^{-3})	1.303, −1.219	0.71, −1.27	4.166, −2.478	1.537, −1.242	1.181, −1.711	1.400, −1.052	0.79, −0.74

Compound	8′	9′	10	12
chemical formula	$C_{19}H_{26}N_5O_{16}ZnTb$	$C_{19}H_{26}N_5O_{16}ZnDy$	$C_{19}H_{26}N_5O_{16}ZnHo$	$C_{19}H_{26}N_5O_{16}ZnTm$
M (g mol^{-1})	804.74	808.27	810.70	814.75
temp (K)	180	293(2)	293(2)	180
wavelength (Å)	0.71073	0.71073	0.71073	0.71073
cryst syst	triclinic	triclinic	triclinic	triclinic
Space group	$P\bar{1}$	$P\bar{1}$	$P\bar{1}$	$P\bar{1}$
a (Å)	9.3675(2)	9.3967(8)	9.3898(7)	9.3366(2)
b (Å)	9.4338(2)	9.5343(8)	9.5319(7)	9.4071(2)
c (Å)	15.9583(4)	16.0729(14)	16.0509(11)	15.8396(4)
α (deg)	103.5820(10)	103.557(7)	103.713(6)	103.613(2)
β (deg)	100.6620(10)	100.567(7)	100.432(6)	100.471(2)
γ (deg)	97.0380(10)	97.521(7)	97.474(6)	97.201(2)
V (Å^3)	1326.66(5)	1353.2(2)	1349.89(17)	1308.86(5)
Z	2	2	2	2
D_c (g cm^{-3})	2.014	1.969	1.980	2.067
μ (mm^{-1})	3.635	3.711	3.883	4.372
F(000)	796	786	788	804
refinement on	F	F^2	F^2	F
goodness of fit	1.070	1.040	1.074	1.0959
final R_1, wR_2	0.0156, 0.0191	0.0434, 0.1105	0.0301, 0.0669	0.0244, 0.0279
$[I > n\sigma(I)]$	$n = 3$	$n = 2$	$n = 2$	$n = 3$
R_1, wR_2 (all data)	0.0184, 0.0199	0.0489, 0.1131	0.0372, 0.0692	0.0271, 0.0287
largest diff. peak and hole (eÅ^{-3})	1.19/−0.53	1.683, −2.604	0.821, −1.421	1.76, −1.96

on their potential importance in magnetic applications,[7] while relatively few have described the photophysical properties of these compounds.[8] It has been shown that the conjugated organic ligands used in these systems, with absorption bands generally at longer wavelengths compared to nonconjugated systems, can act as improved antennae or sensitizers for NIR lanthanide luminescence, enhancing the luminescent properties.[9]

dx.doi.org/10.1021/ic200426w |*Inorg. Chem.* 2011, 50, 5879–5889

In this paper, we report on the synthesis of a series of 13 [$Zn^{II}Ln^{III}$] heterodinuclear complexes containing the valpn^{2-} ligand [H_2valpn = 1,3-propanediylbis(2-iminomethylene-6-methoxy-phenol)]. Their crystal structures and magnetic and optical properties have been investigated. The magnetic studies were performed in order to emphasize the nature of the exchange interaction between Ni^{II} and anisotropic Ln^{III} ions in a series of dinuclear [$Ni^{II}Ln^{III}$] compounds constructed by using the same ligand (see the following paper in this issue). Because the potential application of these compounds as sensors or in light-emitting diodes is extremely important and requires more fundamental research, we studied the luminescence properties in the solid state, by recording the excitation and emission spectra of the compounds. It has been found that the heterodinuclear complexes containing Nd^{III}, Sm^{III}, Tb^{III}, Dy^{III}, and Yb^{III} present the characteristic emissions of these ions.

EXPERIMENTAL SECTION

Materials. The chemicals used, *o*-vanillin, 1,3-diaminopropane, $Zn(NO_3)\cdot 6H_2O$, and $Ln(NO_3)_3\cdot xH_2O$, as well as all of the solvents (THF, acetonitrile) were purchased from commercial sources.

The mononuclear precursor, [Zn(valpn)(H_2O)], was prepared starting from 50 mL of a THF solution containing 20 mmol of *o*-vanillin, to which was added dropwise, under stirring, 10 mmol of 1,3-diaminopropane and then 20 mmol of triethylamine. After 30 min, an aqueous solution (50 mL) containing 10 mmol of $Zn(NO_3)_2\cdot 6H_2O$ was added, and the resulting mixture was stirred for 1 h, while pouring in 200 mL of H_2O, in order to facilitate the precipitation of the mononuclear complex. The pale yellow solid obtained (yield: 75−80%) was then vacuum filtered and dried. IR spectra and elemental analyses were used to characterize the starting material.

The synthesis of the heterodinuclear [$Zn^{II}Ln^{III}$] complexes consists of the addition of 4 mmol of $Ln(NO_3)_3\cdot xH_2O$, under stirring, to a suspension containing 4 mmol of [Zn(valpn)(H_2O)] in 20 mL of acetonitrile. The reaction mixture was stirred for about 30 min. After several days, yellow [$Zn(H_2O)(valpn)Ln^{III}(O_2NO)_3$] ($Ln^{III}$ = La, **1**; Ce, **2**; Pr, **3**; Nd, **4**; Sm, **5**; Gd, **7**; Tb, **8**; Dy, **9**), yellow {[$Zn(ONO_2)(valpn)Ln(H_2O)(O_2NO)_2$]($H_2O$)$_2$} ($Ln^{III}$ = Tb, **8′**; Dy, **9′**; Ho, **10**), orange [$Zn(H_2O)(valpn)Eu((O_2NO)_3$] (**6**), and orange {[$Zn((ONO_2)(valpn)Ln^{III}(H_2O)(O_2NO)_2$]($H_2O$)$_2$} ($Ln^{III}$ = Er, **11**; Tm, **12**; Yb, **13**) crystals of the desired compounds were obtained through the slow vaporization of the solvent. Pertinent crystal data collection and refinement parameters for compounds **1**−**9** and **8′**, **9′**, and **10**−**12** are given in Table 1.

Physical Measurements. UV−vis−NIR spectra were recorded on a JASCO V-670 spectrophotometer using crushed crystals of the compounds.

The photoluminescence (PL) measurements were carried out using a Fluoromax 4P spectrofluorometer (Horiba) operated in both the fluorescence and the phosphorescence mode, using fine crystalline powder obtained by crushing the crystals of the heterodinuclear [$Zn^{II}Ln^{III}$] complexes. The repetition rate of the xenon flash lamp was 25 Hz. The integration window varied between 300 ms and 3 s. The delay after flash varied between 0.03 and 10 ms, and up to 100 flashes were accumulated per data point. The slits were varied from 0.01 to 10 nm in excitation as well as emission. PL decays were measured by using the "decay by delay" feature of the phosphorescence mode. Time resolved emission spectra (TRES) were also recorded by using a nitrogen laser (emission wavelength at 337 nm, a frequency of 20 Hz, model VSL-337ND-S from Spectra-Physics) and an intensified CCD camera (Andor Technology) coupled to a spectrograph (Shamrock 303i, Andor Technology). The TRES were collected using the boxcar technique. The initial gate delay, (delay after laser pulse) was set to 1 μs, and the gate width was adjusted to 50 μs. Laser excited photoluminescence measurements were also performed at liquid nitrogen temperature (80 K). For the low-temperature measurements, the solid state samples were mounted on a coldfinger attached to a liquid nitrogen Dewar. The emission spectra in the NIR spectral region were measured by using a mercury lamp, a Jarrell−Ash 78−460 monochromator, and a liquid nitrogen-cooled JUDSON J16D-M204-R05M-60 Ge detector. Emission and excitation spectra in the VIS spectral range were corrected for the spectral response of the emission and excitation detectors, whereas the emission spectra in the NIR spectral range were not corrected.

The PL decays were analyzed by fitting with a multiexponential function $f(t)$ using the commercial software (OriginPro 8):

$$f(t) = \sum_i^n A_i \exp(-t/\tau_i) + B \quad (1)$$

where A_i is the decay amplitude, B is a constant (the baseline offset), and τ_i is the time constant of the decay i. The average decay times, τ_{av}, were calculated using the following formula:

$$\tau_{av} = \frac{\sum_i^n A_i \tau_i^2}{\sum_i^n A_i \tau_i} \quad (2)$$

X-ray diffraction data for the crystals of compounds **1**, **5**, **6**, **7**, **8**, **9′**, and **10** were collected at 293 K on an IPDS II STOE diffractometer using a graphite-monochromated Mo Kα radiation source (λ = 0.71073 Å). For compounds **3**, **8′**, **9**, and **12**, data were collected at 180 K on an Xcalibur Oxford Diffraction or Apex2 Bruker diffractometer using a graphite-monochromated Mo Kα radiation source (λ = 0.71073 Å) and equipped with Oxford Cryosystems Cryostream Cooler devices. Multiscan absorption corrections were applied. The structures were solved by direct methods and refined by full-matrix least-squares techniques based on F^2 for the compounds **1**, **5**, **6**, **7**, **8**, **9′**, and **10** and on F for the compounds **3**, **8′**, **9**, and **12**, respectively. The non-H atoms were refined with anisotropic displacement parameters. The structures were solved using SHELXS-97 (for the compounds **1**, **5**, **6**, **7**, **8**, **9′**, and **10**) or SIR92 (for the compounds **3**, **8′**, **9**, and **12**) and refined using SHELXL-97 (**1**, **5**, **6**, **7**, **8**, **9′**, and **10**) or CRYSTALS (**3**, **8′**, **9**, and **12**) crystallographic software packages. Hydrogen atoms were refined with riding constraints. Drawings of the molecule were performed with the program Diamond 3. Supplementary X-ray crystallographic data in CIF format have been deposited with the CCDC with the following reference numbers: 794399 (**9**), 794400 (**8′**), 794401 (**12**), 794402 (**3**), 815085 (**5**), 815086 (**8**), 815087 (**9′**), and 815088 (**10**).

X-ray powder diffraction measurements were performed at room temperature on a Shimadzu XRD-7000 diffractometer (Bragg−Brentano geometry) using Cu Kα radiation, operated at 40 kV and 30 mA in the 2θ range 5−30° with steps of 0.01° and a counting time of 24 s/step. The sample was spun at 15 rpm. The results were analyzed using the GSAS software[10a] with an EXPGUI frontend.[10b] Peak shapes were modeled as Thompson, Cox, and Hastings pseudo-Voigt profile functions[10c] with Finger, Cox, and Jephcoat correction for asymmetry due to axial divergence.[10d]

IR spectra were recorded on a GX system 2000 Perkin-Elmer spectrophotometer. Magnetic data were obtained with a Quantum Design MPMS-5 SQUID susceptometer. Magnetic susceptibility measurements were performed in the 2−300 K temperature range in a 0.1 T applied magnetic field, and diamagnetic corrections were applied by using Pascal's constants.

Diffuse reflectance UV−vis−NIR spectra were recorded on a JASCO V-670 spectrophotometer.

RESULTS AND DISCUSSION

The ability of the compartmental ligands derived from *o*-vanillin and various diamines to generate 3d−4f heterometal

dx.doi.org/10.1021/ic200426w |*Inorg. Chem.* 2011, 50, 5879–5889

complexes is well-known.[7] Such a ligand is the Schiff base obtained from the condensation of *o*-vanillin with 1,3-propanediamine, H_2valpn, that we currently use in order to obtain various 3d−4f and 3d−3d′ complexes.[11] Recently, we reported on the quite surprising photophysical properties of the europium derivative $[Zn(H_2O)(valpn)Ln^{III}(O_2NO)_3]$, namely, a strong $^5D_0$ emission of europium obtained by using a 535 nm radiation direct excitation, while the antenna effect is observed only at 80 K.[11b] In this study, a series of heterodinuclear $[Zn(H_2O)(valpn)Ln^{III}(O_2NO)_3]$ (Ln^{III} = La, **1**; Ce, **2**; Pr, **3**; Nd, **4**; Sm, **5**; Eu, **6**; Gd, **7**; Tb, **8**; Dy, **9**) and $[Zn(ONO_2)(valpn)Ln^{III}(H_2O)(O_2NO)_2]\cdot 2H_2O$ (Ln^{III} = Tb, **8′**; Dy, **9′**; Ho, **10**; Er, **11**; Tm, **12**; Yb, **13**) complexes were synthesized by the reaction, in acetonitrile, of stoichiometric amounts of $[Zn(valpn)(H_2O)]$ and $Ln(NO_3)_3\cdot xH_2O$. The crystal structures and luminescence properties of complexes **1**, **6**, and **7** have been discussed in a preceding paper,[11b] but since their magnetic properties are presented in this work, we inserted their crystallographic data in Table 1.

Description of Structures. The X-ray diffraction studies showed that all of the new complexes are heterodinuclear compounds. The determination of the lattice parameters indicated two structural types: type I (for compounds **1**−**9**) and type II (**8′**, **9′**, **10**−**13**; see Table 1), which are correlated to the position of the rare earth ion in the 4f series and, therefore, to its ionic size and Lewis acidity.

The heterodinuclear complexes belonging to type I have the general formula $[Zn(H_2O)(valpn)Ln^{III}(O_2NO)_3]$ (Ln^{III} = La, **1**; Ce, **2**; Pr, **3**; Nd, **4**; Sm, **5**; Eu, **6**; Gd, **7**; Tb, **8**; Dy, **9**) and crystallize in the $P2_1/c$ monoclinic space group. The X-ray crystal structures were solved for the **1**, **3**, **5**, **6**, **7**, **8**, and **9** complexes, while the structures for compounds **2**, and **4** were ascertained by recording the lattice parameters. The structures of type I consist of a neutral dinuclear complex of formula $[Zn(H_2O)(valpn)Ln^{III}(O_2NO)_3]$. As an example, we discuss here the structure of the samarium derivative, **5** (Figure 1).

The zinc ion has a square pyramidal environment, with a N_2O_2 tetragonal base formed by the donor atoms of the organic ligand [Zn1−N1 = 2.049(6); Zn1−N2 = 2.047(6); Zn1−O2 = 2.035(4); Zn1−O3 = 2.031(4) Å] and an apical aqua ligand [Zn1−O14 = 2.055(6) Å]. The lanthanide ion is located in the open compartment, being surrounded by 10 oxygen atoms: two phenolato and two methoxy oxygen atoms arising from the Schiff-base [Sm1−O1 = 2.556(4); Sm1−O2 = 2.360(4); Sm1−O3 = 2.409(4); Sm1−O4 = 2.563(4) Å] and two oxygen atoms from each of the three chelating nitrato ions [Sm1−O5 = 2.490(5); Sm1−O7 = 2.479(6); Sm1−O8 = 2.522(5); Sm1−O10 = 2.523(4); Sm1−O11 = 2.586(5); Sm1−O12 = 2.567(5) Å]. Selected bond distances for type I complexes are gathered in Table S1 in the Supporting Information.

At the supramolecular level, the dinuclear units interact through hydrogen bonds established between the oxygen atom of the aqua ligand (O14) and the oxygen atom (O13) of one nitrato ligand belonging to a neighboring complex, resulting in a supramolecular chain (Figure 2). Intermolecular distances are long enough to preclude any significant magnetic exchange interactions between the paramagnetic metal ions. The shortest Sm···Sm separation is Sm1···Sm1‴ = 8.306 Å; ‴ = x, 0.5 − y, 0.5 + z).

The second structural type consists of complexes with the general formula $[Zn(ONO_2)(valpn)Ln^{III}(O_2NO)_2(H_2O)]\cdot 2H_2O$ (Ln^{III} = Tb, **8′**; Dy, **9′**; Ho, **10**; Er, **11**; Tm, **12**; Yb, **13**) crystallizing in the $P\bar{1}$ triclinic space group. The single-crystal X-ray structures were solved for the **8′**, **9′**, **10**, and **12** complexes, while lattice parameters confirmed **11** and **13** to exhibit isomorphous structures. The crystallographic investigations revealed that type II compounds consist of a

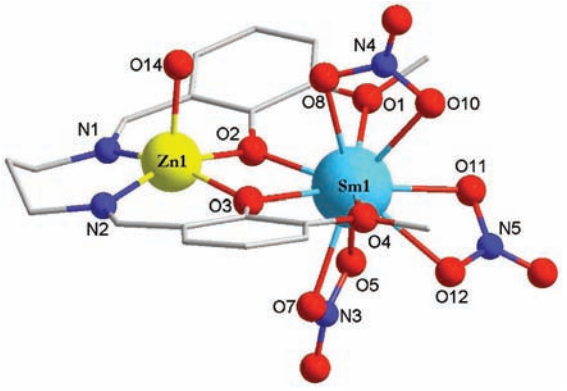

Figure 1. View of the molecular structure for $[Zn(H_2O)(valpn)Sm(O_2NO)_3]$.

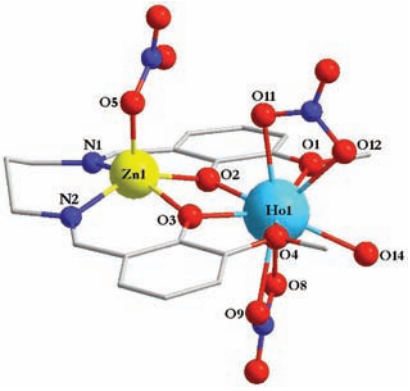

Figure 3. View of the molecular entity $[Zn(ONO_2)(valpn)Ho(O_2NO)_2(H_2O)]$.

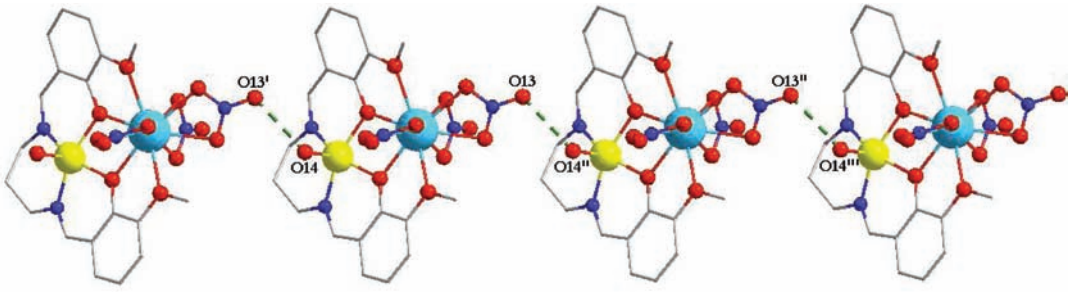

Figure 2. Packing diagram for compound **5** showing the formation of the supramolecular chains (′ = x, y, 1 + z; ″ = x, y, −1 + z; ‴ = x, y, −2 + z).

dx.doi.org/10.1021/ic200426w |*Inorg. Chem.* 2011, 50, 5879–5889

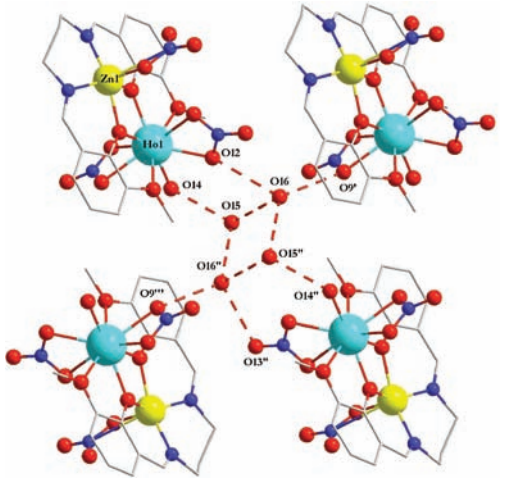

Figure 4. View of the tetranuclear water cluster formed within the crystalline structure of **10** [O16···O15 = 3.008; O16···O15' = 2.783 Å]. (′ = 2 − *x*, 2 − *y*, −*z*.)

neutral dinuclear complex of formula $[Zn(ONO_2)(valpn)Ln^{III}(O_2NO)_2(H_2O)]$ and crystallization water molecules.

A special case within the series of dinuclear complexes is the $[Zn^{II}Dy^{III}]$ system. Two types of crystals, belonging to either type I or type II structures, respectively, **9** and **9′**, have been isolated. Obviously, the size of Dy^{III} allows this ion to adopt the two structural arrangements. X-ray powder diffraction was performed on the powder collected from one beaker in which the $[Zn^{II}Dy^{III}]$ system was obtained. The comparison (Figure S1 in the Supporting Information) of the experimental diffraction pattern with the simulated ones for each phase was made using the profile parameters determined from the standard silicon sample and introducing preferred orientation effects: (040) and (011) for the monoclinic complex (**9**) and (100) and (002) for the triclinic one (**9′**). The analysis of the diffractograms confirms the presence of both phases, with **9′** as a major component (Figure S1 in the Supporting Information). The same situation was observed with the Tb^{III}−Zn^{II} system (complexes **8** and **8′**).

The type II structure will be illustrated using the Ho^{III} derivative, **10**, whose molecular unit is shown in Figure 3. The zinc ion displays a square pyramidal environment, with a N_2O_2 tetragonal base formed by the donor atoms of the organic ligand [Zn1−N1 = 2.063(2); Zn1−N2 = 2.066(2); Zn1−O2 = 2.0626(19); Zn1−O3 = 2.0703(17) Å] and an apical nitrato ligand [Zn1−O5 = 2.047(2) Å].

The lanthanide ion is located in the open compartment, being surrounded by nine oxygen atoms: two phenolato and two methoxy oxygen atoms arising from the Schiff base [Ho1−O1 = 2.451(2); Ho1−O2 = 2.2704(17); Ho1−O3 = 2.2663(19); Ho1−O4 = 2.455(2) Å], four oxygen atoms arising from the two chelating nitrato ions [Ho1−O8 = 2.453(2); Ho1−O9 = 2.484(6); Ho1−O11 = 2.483(2); Ho1−O12 = 2.414(2) Å], and the oxygen atom of one aqua ligand [Ho1−O14 = 2.374(2) Å]. Selected bond distances for type II complexes are gathered in Table S2 in the Supporting Information.

A complex 3-D supramolecular architecture is formed through the interplay of various hydrogen bonds established between the lattice water molecules, the aqua ligands, and the oxygen atoms of the chelating and monodentate nitrato ligands. It is worthy to note that the crystallization water molecules form tetrameric clusters (Figure 4). The shortest Ho···Ho separation (Ho1···Ho1″ = 8.011 Å, ″ = 1 − *x*, 2 − *y*, −*z*) is long enough to prevent any significant magnetic exchange interactions between the lanthanide ions.

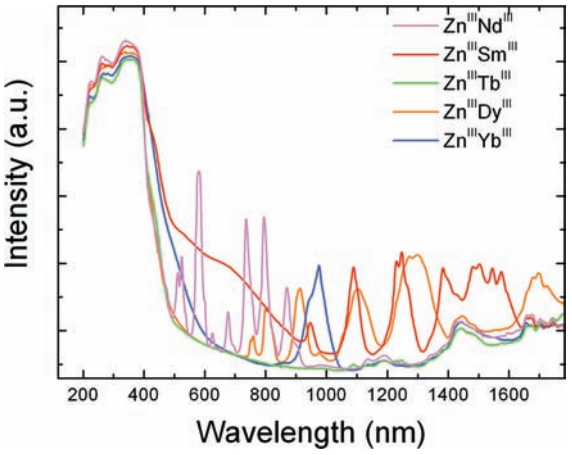

Figure 5. UV−vis−NIR absorption spectra of the luminescent $[Zn^{II}Ln^{III}]$ heterodinuclear complexes.

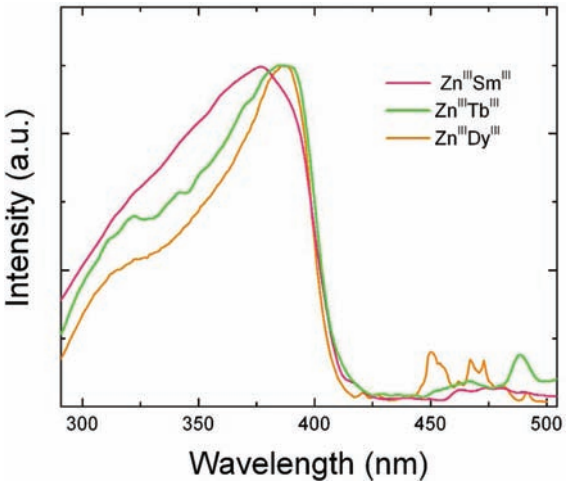

Figure 6. PL excitation spectra of $[Zn^{II}Sm^{III}]$, $[Zn^{II}Tb^{III}]$ and $[Zn^{II}Dy^{III}]$ complexes (λ_{em} = 594, 542, and 574 nm, respectively).

UV−vis−NIR Absorption Spectra. The heterodinuclear $[Zn^{II}Ln^{III}]$ complexes display a structured absorption band in the UV, corresponding to π−π^* transitions, with three peaks with increasing intensity as follows: 222 nm < 260 nm < 340−375 nm, a shoulder at about 430 nm, and a cutoff at ∼500 nm (Figure 5). Sharp lines in the spectral range of ∼450−1600 nm were attributed to the Ln^{III} f−f absorption transitions. No significant differences were observed in the 200−450 nm spectral region, as the Ln^{III} ion is varied among the $[Zn^{II}Ln^{III}]$ series (Ln^{III} = Nd^{III}, Sm^{III}, Gd^{III}, Tb^{III}, Dy^{III}, Yb^{III}).

Photoluminescence of $[Zn^{II}Sm^{III}]$, $[Zn^{II}Tb^{III}]$, and $[Zn^{II}Dy^{III}]$ Complexes. The photoluminescence (PL) excitation spectrum of $[Zn(H_2O)(valpn)Sm(O_2NO)_3]$ (Figure 6) was measured on the strongest vis emission of Sm^{III} (λ_{em} = 594 nm), corresponding to the $^4G_{5/2}$−$^6H_{5/2}$ transition (Figure 7a). The spectrum is dominated by a broad 390 nm peaked band which corresponds to the excitation through the $^1\pi\pi^*$ ligand state (see also Figure 5).

dx.doi.org/10.1021/ic200426w |*Inorg. Chem.* 2011, 50, 5879–5889

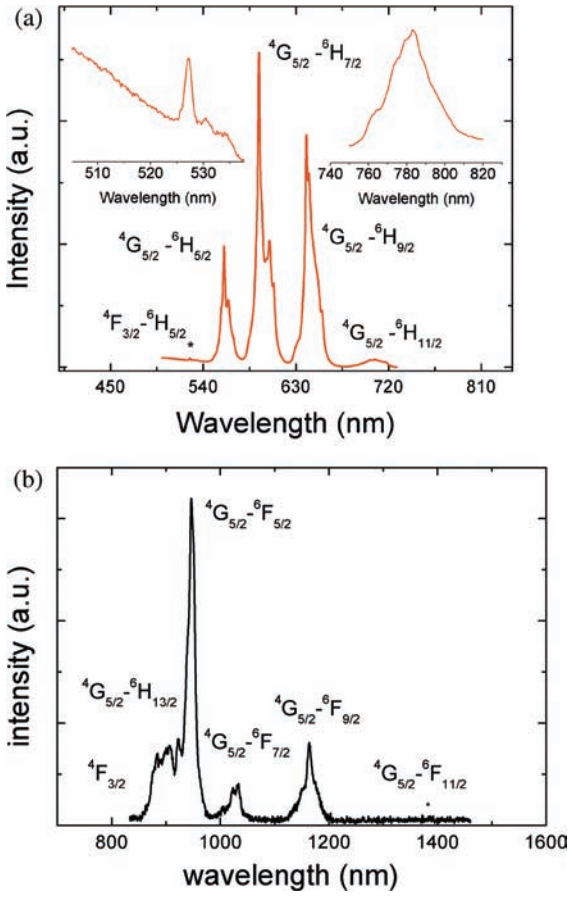

Figure 7. (a) PL spectrum of $[Zn^{II}Sm^{III}]$ in the vis spectral region (λ_{ex} = 390 nm). Inset left: PL emission in the spectral region of $^4F_{3/2}-^6H_{5/2}$ transition. Inset right: PL emission in the spectral region of $^4G_{5/2}-^6H_{13/2}$ transition. (b) PL spectrum of $[Zn^{II}Sm^{III}]$ in the NIR spectral region following UV excitation.

Weak absorptions within the spectral range of 450−540 nm were assigned to the mixing of $^6H_{5/2}-^4F_{5/2}$, $^6H_{5/2}-^4I_{13/2}$, $^6H_{5/2}-^4I_{11/2}$, $^6H_{5/2}-^4M_{15/2}$, $^6H_{5/2}-^4I_{9/2}$, and $^6H_{5/2}-^4F_{3/2}$ Sm^{III} transitions. The vis absorption transitions are not detectable in the UV−vis−NIR spectrum in contrast with the strong spin-allowed ($\Delta S = 0$) NIR transitions (among these, the $^6H_{5/2}-^6F_{9/2}$ at 1108 nm and $^6H_{5/2}-^6F_{7/2}$ at 1264 nm are the most intense).

A strong, reddish emission of $[Zn^{II}Sm^{III}]$ was observed by the naked eye following excitation with a standard UV lamp (λ_{ex} = 365 nm). The four characteristic bands of Sm^{III} originated from the $^4G_{5/2}$ state to the ^6H_J (J = 5/2, 7/2, 9/2, 11/2) at about 560, 594, 640, and 710−720 nm (Figure 7a), and their peak normalized integrated intensities were determined at 3.44, 10.2, 8.95, and 0.6, respectively.

With an increase in the integration time, the emission of $^4G_{5/2}-^6H_{13/2}$ at about 784 nm could also be detected. Among the two magnetic dipole allowed transitions, $^4G_{5/2}-^6H_{5/2}$ and $^4G_{5/2}-^6H_{7/2}$, the former has a predominant magnetic dipole character. A value of 2.6 was measured for the intensities ratio of the electric dipole allowed hypersensitive $^4G_{5/2}-^6H_{9/2}$ and the magnetic dipole $^4G_{5/2}-^6H_{5/2}$ transition, respectively, supporting a moderate polarizable environment at the ion's site.[12] For comparison, an asymmetry value of 4.6 was found for the intensity ratio of the hypersensitive to magnetic dipole $^5D_0-^7F_2/^5D_0-^7F_1$ transitions of Eu^{III} in the isostructural $[Zn^{III}Eu^{III}]$ complex (**6**).[11b] The relative intensities of the $^4G_{5/2}-^6H_{5/2}$, $H_{7/2}$, and $^6H_{9/2}$ transitions vary significantly across the Sm^{III} complexes with Schiff ligands;[13] hence, their ratio may be informative for the polarizability or symmetry effects at the lanthanide's site. For any symmetry lower than cubic, the maximum number of Stark components for the Sm^{III} ion is $J + 1/2$ (Kramer's degeneracy). At room-temperature, the luminescence may originate from all three crystal-field levels of $^4G_{5/2}$, giving nine lines for the $^4G_{5/2}-^6H_{5/2}$ emission, among which only six could be resolved. The PL decay of Sm^{III} measured at 594 nm is single exponential (τ = 40 ± 2 μs), indicating a single coordination environment, which is in perfect agreement with the X-ray data (see also Figure 9). The weak intensity peak at 527 nm is assigned to the $^4F_{3/2}-^6H_{5/2}$ transition and has a decay time of 38 ± 5 μs, which comes close to that of the $^4G_{5/2}$ level. Such a result together with the small energy gap (about 1100 cm^{-1}) above the $^4G_{5/2}$ level demonstrates that the $^4F_{3/2}$ level is thermally populated at 300 K.

We briefly recall that the Sm^{III} complex **5** crystallizes as a type I compound (Table 1), being surrounded by 10 oxygen atoms: two phenolato and two methoxy oxygen atoms arising from the Schiff base and two oxygen atoms from each of the three chelating nitrato ions (Figure 1). The absence of the water molecules in the first coordination sphere of Sm^{III} is a necessary requirement for strong emission, especially in the NIR region. Indeed, following excitation into UV, near-infrared emission of **5** was also observed (Figure 7b), being assigned to the transitions between the $^4G_{5/2}$ excited state and the ^6F_J levels (J = 5/2 to 11/2). The $^4G_{5/2}-^6F_{5/2}$ transition at 950 nm is the most intense. The line structure observed at shorter wavelengths (higher energy) of the $^4G_{5/2}-^6F_{5/2}$ transitions is due to the interferences from the $(^4F_{3/2}, ^4G_{5/2})-^6H_{15/2}$ transitions.

According to a recent model,[14] the ligand-to-metal energy transfer occurs via the triplet states $^3\pi\pi^*$ of the ligand to the $^4G_{5/2}$ level of Sm^{III}, and the mechanism is of the exchange type. The location of the triplet state at about 550 nm (ca. 18 180 cm^{-1})[11b] is only slightly higher than the emissive Sm^{III} level (ca. 17 850 cm^{-1}), which allows, in principle, the back-transfer of excitation from $^4G_{5/2}$ to the triplet level of the ligand. However, its strong emission and relatively long lifetime do not sustain a sizable value of the back-transfer. Further, no intraligand fluorescence was observed, which supports an efficient energy transfer from the triplet state of the ligand to the Sm^{III} ion (some weak ligand-related emission could however be detected, Figure 7a, inset), but its contribution to the total emission is negligible. In fact, the value of the triplet energy could be actually higher than 18 180 cm^{-1}, as it was inferred from the maximum of the broad, unstructured emission of the Gd^{III} complex at 80 K (and not from the 0−0 vibrational transition energy).[11b]

Similar to $[Zn^{II}Sm^{III}]$, strong sensitization of terbium emission via the ligand was obtained for the $[Zn^{II}Tb^{III}]$ complex (Figure 6). The large peak at 380−390 nm with a spectral shoulder at 320 nm was assigned to the ligand absorption, while the weak, narrow line at 490 nm was assigned to the terbium $^7F_6-^5D_4$ transition. The PL spectrum shows, besides the most intense transition at 542 nm, three other peaks at about 490 nm ($^5D_4-^7F_6$), 586 nm ($^5D_4-^7F_4$), and 624 nm ($^5D_4-^7F_3$). No ligand related fluorescence was detected, supporting the efficient energy transfer from the ligand to the terbium $^5D_4$ excited state. The increase of the spectral resolution or lowering of the measurement temperature down to 80 K (Figure 8, inset) did not significantly resolve the Stark structure of the emission lines.

dx.doi.org/10.1021/ic200426w |*Inorg. Chem.* 2011, 50, 5879–5889

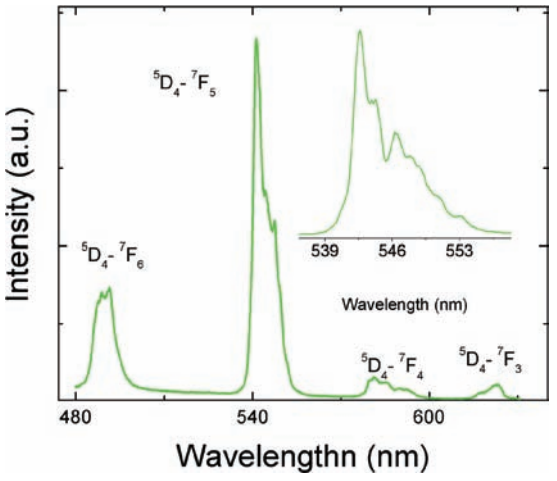

Figure 8. PL spectrum of the $[Zn^{II}Tb^{III}]$ complex 300 K (λ_{ex} = 390 nm). Inset: Zoomed PL spectrum around $^5D_4-^7F_5$ following laser excitation at 337 nm (80 K).

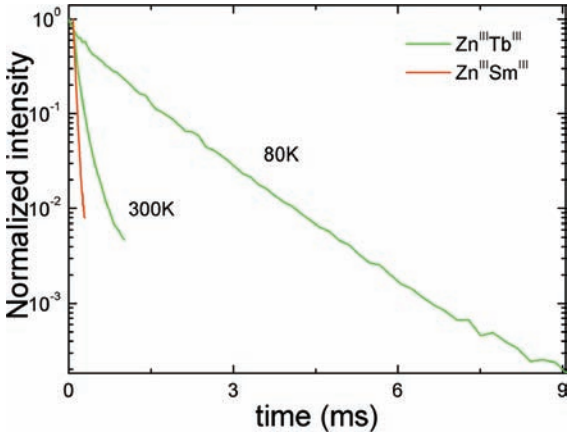

Figure 9. Comparison between the PL decays of $[Zn^{III}Tb^{III}]$ measured at 80 and 300 K (λ_{ex} = 337 nm, λ_{em} = 542 nm). The PL decay of $[Zn^{III}Sm^{III}]$ is also included (λ_{ex} = 390 nm and λ_{em} = 594 nm).

The Stark structure within the $^5D_4-^7F_5$ transition is further complicated, as terbium complex crystallizes in both type I and II geometries (as **8** and **8′**, Table 1).

As expected from the X-ray structural data, the PL decays of $[Zn^{II}Tb^{III}]$ were nonexponential at both room and liquid nitrogen temperatures (Figure 9) being satisfactorily fitted with two exponentials (eq 1). At room-temperature, the decay times (μs) and amplitudes (%) were 50 ± 1 μs (80 ± 0.8) and 145 ± 3 μs (20 ± 0.3). At 80 K, the amplitudes and the decay times changed to 300 ± 10 μs (25 ± 2) and 1020 ± 5 μs (75 ± 2).

The average PL lifetime of only 96 ± 1 μs (eq 2) measured at room-temperature supports strong nonradiative quenching of the metastable $^5D_4$ state emission, as the terbium PL lifetimes in complexes with organic ligands usually range in the miili-second domain. We briefly recall that compared to type I $[Zn(H_2O)(valpn)Tb(O_2NO)_3]$ (**8**), where terbium emission is fully protected against −OH deactivators, the type II terbium complex (**8′**) consists of a neutral dinuclear complex of formula $[Zn(ONO_2)(valpn)Tb^{III}(O_2NO)_2(H_2O)]$ and crystallization water molecules. The terbium ion is surrounded, aside from the eight oxygen atoms of the two phenolato and two methoxy

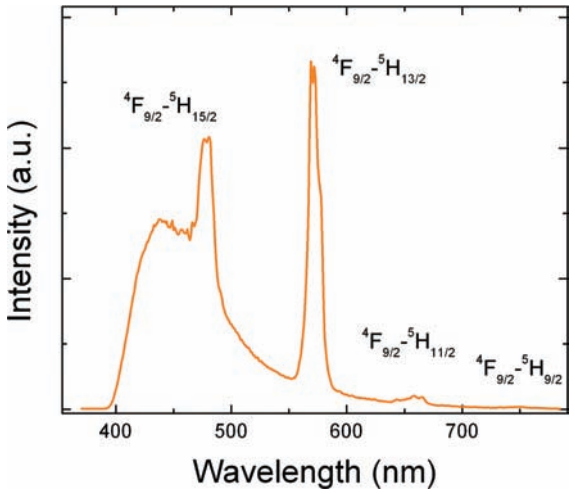

Figure 10. PL spectrum of the $[Zn^{II}Dy^{III}]$ complex around the $^4F_{9/2}-^5H_{15/2}$, $^5H_{11/2}$, $^5H_{9/2}$ transitions (λ_{ex} = 390 nm).

oxygen atoms arising from the Schiff base and four oxygen atoms arising from the two chelating nitrato ions, by the oxygen atom of one aqua ligand. However, the temperature-independent vibrational coupling of the $^5D_4$ level of terbium (energy gap[15] of ca. 14 800 cm^{-1}) occurs with the fourth harmonic of a bound −OH oscillator ($\nu_{OH} \sim 3300-3500$ cm^{-1}), and thus the presence of a single water molecule in the inner coordination sphere of terbium is not expected to induce a strong reduction of the PL lifetime. The increase of the average lifetime by almost 1 order of magnitude, i.e., from τ_{av} = 96 μs ± 2 (300 K) to τ_{av} = 955 ± 5 (80 K), confirmed the dominant contribution of a temperature- *dependent* vibrational quenching. Most probably, the nonradiative deactivation of the terbium emitting state in the $[Zn^{II}Tb^{III}]$ complex is dominated by an efficient back-energy transfer process from the $^5D_4$ level of terbium to the triplet states of the ligand. For **8**, the energy of the ligand triplet state (ca. 18 180 cm^{-1})[11b] lies ca. 2200 cm^{-1} below the $^5D_4$ level of terbium (20 408 cm^{-1}), while for **8′** it was not determined. Similar strong sensitization effects for the ligand triplet levels located well below the $^5D_4$ energy were reported elsewhere.[14] In these cases, the singlet pathway of the emission sensitization may be effective, as proposed for terbium complexes with several Schiff base ligands.[16b−d]

The PL excitation spectrum of the $[Zn^{II}Dy^{III}]$ complex (Figure 6) was measured using the strongest emission transition, $^4F_{9/2}-^5H_{13/2}$, of dysprosium (λ_{em} = 574 nm), Figure 10. Similar to the Sm^{III} and Tb^{III} complexes, the excitation spectrum contains a large absorption band peaked at 380−390 nm. The weak absorption bands detected in the spectral range of 410−490 nm were assigned to the dysprosium $^5H_{15/2}-^4G_{11/2}$, $^5H_{15/2}-^4I_{11/2}$, and $^5H_{15/2}-^4F_{9/2}$ transitions. The vis absorption transitions are not detectable in the UV−vis−NIR spectrum in contrast to the strong spin-allowed NIR transitions (among these, $^6H_{15/2} \rightarrow (^6H_{9/2}, ^6F_{11/2})$ at about 1260 nm are the most intense), Figure 5.

Following excitation at 390 nm, relative intense emissions at 480 nm ($^4F_{9/2}-^5H_{15/2}$) and 574 nm ($^4F_{9/2}-^5H_{13/2}$) were observed along with the much weaker emissions at 635−675 nm ($^4F_{9/2}-^5H_{11/2}$) and 730−770 nm ($^4F_{9/2}-^5H_{9/2}$), the latter observed under increased spectral resolution (Figure 10). The broad emission centered at about 430−440 nm was completely quenched following a few microsecond delay, being assigned to the ligand-related $^1\pi\pi^*$ fluorescence.

dx.doi.org/10.1021/ic200426w |*Inorg. Chem.* 2011, 50, 5879–5889

The Dy^{III} PL decay (λ_{em} = 574 nm, λ_{ex} = 380 nm) could be satisfactorily fitted with a two-exponential function, resulting in an average lifetime of 16 ± 2 μs (eq 2). The nonexponential shape of PL decay was assigned to the coexistence of the type I (**9**) and II (**9′**) complexes, with type II as a major component, as inferred from the X-ray data (Figure S1 in the Supporting Information). A detailed analysis of the decay was not performed due to the measured low signal-to-noise ratio.

The metastable level of Dy^{III} ($^4F_{9/2}$) is situated at about 20 830 cm^{-1} above the ground state. To our knowledge, for dysprosium, there are no imposed thresholds values for the difference ΔE (T1 − $^4F_{9/2}$), which should optimize the IET from the ligand to Dy^{III} excited levels. The presence of a relative intense ligand emission in the emission spectrum of [$Zn^{III}Dy^{III}$] (which accounts for ca. 55% of the total emission intensity) together with the relative contribution of the f−f absorption transitions in the Dy^{III} excitation spectrum (Figure 6) demonstrates a relatively less efficient energy transfer than for the Sm^{III} complex. The energy gap for the Dy^{III} (which is similar to that of Sm^{III} at ∼7500 cm^{-1}) can be efficiently bridged by second-order nonradiative processes involving the −OH vibrational states. As the major Dy^{III} species is of type II (**9′** with one water molecule directly bound to Ln^{III} ion), this can explain its shorter lifetime (16 ± 2 μs) compared to that of **5** (PL lifetime of 40 ± 2 μs). The values of the PL lifetimes for Sm^{III}, Dy^{III}, and Tb^{III} are among the few reported for the heterodinuclear [$Zn^{II}Ln^{III}$] complexes with Schiff ligands.

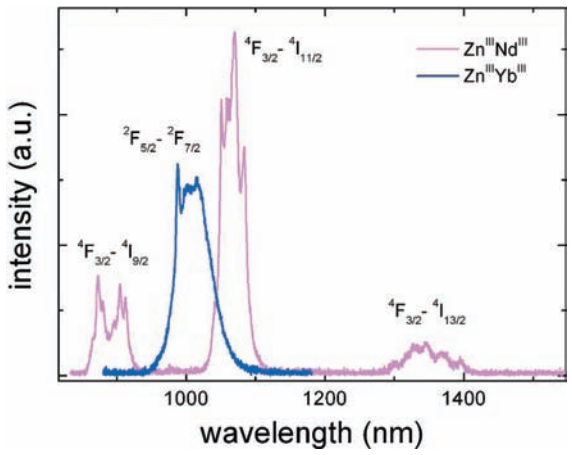

Figure 11. NIR emission (uncorrected) spectra of [$Zn^{II}Nd^{III}$] and [$Zn^{II}Yb^{III}$] complexes following UV excitation.

Photoluminescence of [$Zn^{II}Nd^{III}$], [$Zn^{II}Yb^{III}$], and [$Zn^{II}Er^{III}$] Complexes. Besides vis emitting lanthanide's ions, Schiff base ligands can act as efficient antenna for the NIR emitting ions (Nd^{III}, Yb^{III}, Er^{III}).[9] Among these ions, Nd^{III} displays sensitized NIR emission in a wide range of complexes with Schiff ligands, whose properties may be modulated via the anion inducement.[17]

[$Zn^{II}Nd^{III}$] is a type I compound and emits in the NIR region of the spectrum, at around 900 nm ($^4F_{3/2}$−$^4I_{9/2}$, with the $^4I_{9/2}$−$^4F_{3/2}$ absorption being detected in the UV−vis−NIR spectrum, Figure 5), 1065 nm ($^4F_{3/2}$−$^4I_{11/2}$), and 1330 nm ($^4F_{3/2}$−$^4I_{13/2}$), Figure 11. Seven lines could be detected with $^4F_{3/2}$−$^4I_{9/2}$ transition from a total of 10. However, emission lines below 900 nm may be assigned interference with the $^2H_{5/2}$ and $^4F_{5/2}$→ $^4I_{9/2}$ transitions induced via the thermalization effect. For the Nd^{III} complexes with similar Schiff ligands, both the singlet and the triplet states are usually considered donors for the excitation energy from the ligand to the lanthanide's excited states.[9g]

The Yb^{III} ion has only one excited state, $^2F_{5/2}$, which is about 10 200 cm^{-1} above the ground state, $^2F_{7/2}$ (the $^2F_{7/2}$−$^2F_{5/2}$ absorption transition is detected as a relatively intense ∼978 nm centered band in the absorption spectrum, Figure 5). Several sensitization mechanisms for Yb(III) emission have been proposed but will not be discussed here.[18] The emission spectrum of type II {[Zn(ONO_2)(valpn)Yb(H_2O)(O_2NO)$_2$](H_2O)$_2$} complex **13′** (Figure 11) displays a band with a sharp main component at 978 nm corresponding to 0-phonon transition and broader components at longer wavelengths (lower energy), which were assigned to the inter-Stark $^2F_{5/2}$−$^2F_{7/2}$ transitions. The NIR emission (corresponding to the $^4I_{13/2}$−$^4I_{15/2}$ transition at about 1530 nm or 6500 cm^{-1}) of type II {[Zn(ONO_2)(valpn)Er(H_2O)(O_2NO)$_2$](H_2O)$_2$} complex **11′** could not be detected using similar conditions of UV excitation. Although both Er^{III} and Yb^{III} in **11** and **13**, respectively, have one water molecule directly bound to the lanthanide ion, the vibrational quanta necessary to match the energy gap is ∼3 for the Yb^{III} complex and ∼2 for the Er^{III} complex. Therefore, strong nonradiative quenching via the second order −OH vibrational coupling may explain the absence of the Er^{III} emission in **11.**

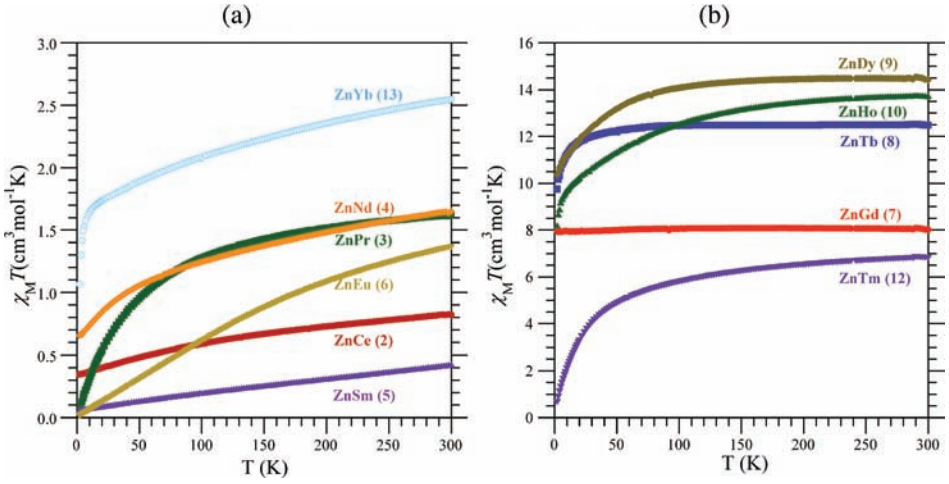

Figure 12. Variation of $\chi_M T$ product for compounds **2**−**6** and **13** (a) and **7**−**12** (b).

dx.doi.org/10.1021/ic200426w |*Inorg. Chem.* 2011, 50, 5879–5889

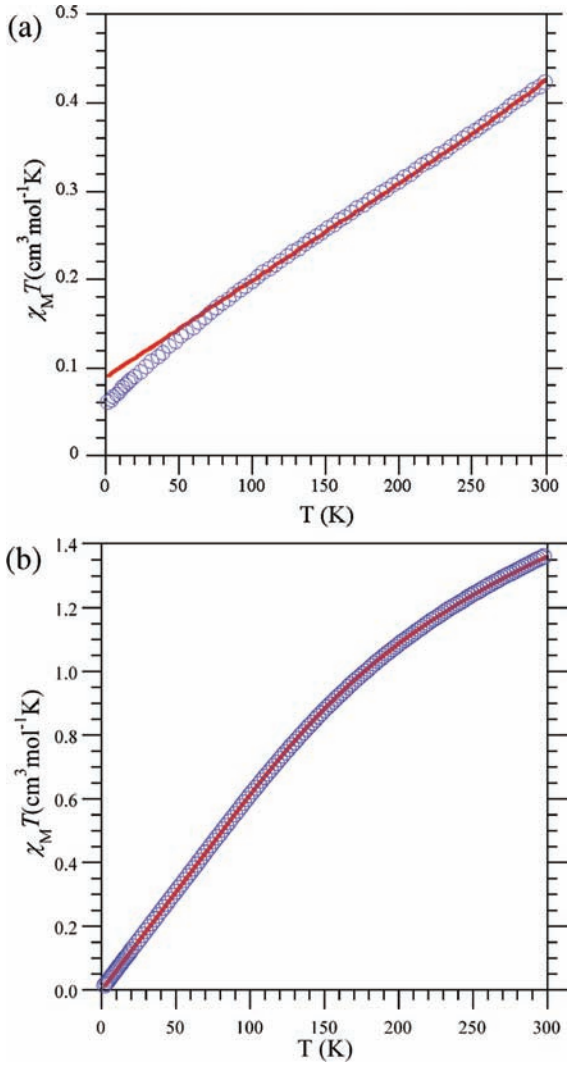

Figure 13. Experimental (○) and calculated (—) temperature dependence of $\chi_M T$ for **5** (a) and **6** (b).

Magnetic Properties. The magnetic properties of compounds **2**−**13** have been investigated using powders of crushed crystals dispersed in grease to avoid orientation in the field.

The room temperature values of the $\chi_M T$ product for the heterodinuclear complexes **2**−**13** are presented in Table S3 (Supporting Information). In the case of the complexes containing Ln^{III} ions with a large energetic separation between the ground state and the first excited state (**2**−**4**, and **7**−**13**), only this ground state is thermally populated at room temperature, and the magnetic susceptibility was calculated using eq 3:[6a]

$$\chi_M = (Ng_J^2\beta^2/3kT)J(J+1) \quad (3)$$

where

$$g_J = 3/2 + [S(S+1) - L(L+1)]/2J(J+1)$$

For the gadolinium derivative (**7**), $g = 2$, $L = 0$, and therefore $J = S$. The $^8S_{7/2}$ ground state is located about 10^4 cm^{-1} below the first excited state.[19] The magnetic data perfectly follow the $\chi_M T = 21N\beta^2/k$ Curie law, as expected (Figure 12b).

For the other complexes, the $\chi_M T$ product decreases continuously as the temperature is lowered, because of the depopulation of the Stark levels.[20]

The complexes of Sm^{III} and Eu^{III} are special cases. The first excited states of these two lanthanide ions lay very close to their ground states, so they are thermally populated even at room temperature. As a consequence, the values reached by $\chi_M T$ in the high temperature domain are much above those given in eq 3. For **5**, $\chi_M T$ is 0.42 cm^3 mol^{-1} K at 300 K and steadily decreases as the temperature is lowered to tend to the low-temperature limit of $(\chi_M T)_{LT} = 0.09$ cm^3 mol^{-1} K predicted by the theory. For the Eu^{III} derivative **6**, $\chi_M T$ continuously decreases as the temperature is lowered and tends to a value very close to zero as T approaches 0 K. The magnetic behavior for both derivatives can be modeled to evaluate their respective spin−orbit coupling parameters.

The ^6H ground term for Sm^{III} is split by spin−orbit coupling into six levels, whose energies increase from $^6H_{5/2}$ to $^6H_{15/2}$ (cf. above, PL section).[19] The spin−orbit coupling parameter is on the order of 200 cm^{-1}, and therefore the first excited state of Sm^{III} ($^6H_{7/2}$) is not very well separated from the ground state, being populated at room temperature and above. The temperature dependence of $\chi_M T$ is nearly linear over the whole temperature range, as also shown by Kahn et al. For temperatures approaching absolute zero, $\chi_M T$ decreases up to the point it reaches the low-temperature limit $(\chi_M T)_{LT} = 0.09$ cm^3 mol^{-1}K predicted by the theory. Taking into account the six states arising from ^6H, the magnetic susceptibility is expressed as[19]

$$\chi_M = (N\beta^2/3kTx)[(a_1x + b_1) + (a_2x + b_2)\,e^{-7x/2} + (a_3x + b_3)\,e^{-8x} + (a_4x + b_4)\,e^{-27x/2} + (a_5x + b_5)\,e^{-20x} + (a_6x + b_6)\,e^{-55x/2}]/[3 + 4\,e^{-7x/2} + 5\,e^{-8x} + 6\,e^{-27x/2} + 7\,e^{-20x} + 8\,e^{-55x/2}] \quad (4)$$

with $a_1 = 2.143$, $b_1 = 7.347$, $a_2 = 42.92$, $b_2 = 1.641$, $a_3 = 283.7$, $b_3 = -0.6571$, $a_4 = 620.6$, $b_4 = -1.9400$, $a_5 = 1122$, $b_5 = -2.835$, $a_6 = 1813$, and $b_6 = -3.556$. x is defined as $x = \lambda/kT$, where λ is the spin−orbit coupling parameter. The best fit of this expression to the experimental behavior was obtained for $\lambda = 208$ cm^{-1} (Figure 13a).

Likewise, the ground state of Eu^{III} (^7F) is split by the spin−orbit coupling into seven ^7F_J states, with energies that increase from $^7F_0$ to $^7F_6$. Since the spin−orbit coupling parameter (λ) is small enough for the first excited states to be thermally populated, the temperature dependence of the magnetic susceptibility is given by eq 5.[19] At room-temperature, a significant fraction (ca. 30%) of europium ions are in the first excited state $^7F_1$, which was supported by the presence of the $^7F_1$−$^5D_0$ absorption line in the excitation spectrum of europium emission.[11b] The best fit of this expression to the experimental behavior of **6** was obtained for $\lambda = 339$ cm^{-1} (Figure 13b).

$$\chi_M = (N\beta^2/3kTx)[24 + (27x/2 - 3/2)\,e^{-x} + (135x/2 - 5/2)\,e^{-3x} + (189x/2 - 7/2)\,e^{-6x} + (405x/2 - 9/2)\,e^{-10x} + (1485x/2 - 11/2)\,e^{-15x} + (2457x/2 - 13/2)\,e^{-21x}]/[1 + 3\,e^{-x} + 5\,e^{-3x} + 7\,e^{-6x} + 9\,e^{-10x} + 11\,e^{-15x} + 13\,e^{-21x}] \quad (5)$$

Conclusions. The excitation spectra of Sm^{III}, Tb^{III}, and Dy^{III} in [$Zn^{II}Ln^{III}$] complexes display ligand-centered bands, thus confirming the ligand-to-metal energy transfer.

dx.doi.org/10.1021/ic200426w |*Inorg. Chem.* 2011, 50, 5879–5889

For the strongest luminescent Sm^{III} complex, a single coordination environment was determined from the X-ray data and the monoexponential PL decay (lifetime of 40 μs). In contrast with Sm^{III}, the emission spectra and the excited states of the more or less luminescent Tb^{III} and Dy^{III} complexes, respectively, are shaped by the presence of two coordination geometries and the excitation back-transfer from the lanthanide's excited states to the triplet state of the ligand. The detection of relatively intense near-infrared emission for $[Zn^{II}Nd^{III}]$, $[Zn^{II}Sm^{III}]$, and $[Zn^{II}Yb^{III}]$ evidences that the valpn ligand constitutes an efficient antenna for both vis and NIR emission of the lanthanides ions. The magnetic properties for these $[Zn^{II}Ln^{III}]$ derivatives are characteristic for the paramagnetism of the corresponding lanthanide ions. They will be used in a further study as references for the intrinsic contribution of the Ln^{III} ions to allow access to the exchange interactions taking place in related exchange coupled dimetallic $[Ni^{II}Ln^{III}]$ compounds.

■ ASSOCIATED CONTENT

Supporting Information. Experimental and simulated powder XRD patterns for the $[Zn^{II}Dy^{III}]$ sample and for each phase (**9** and **9′**). Supplementary X-ray crystallographic data in CIF format. This material is available free of charge via the Internet at http://pubs.acs.org.

■ AUTHOR INFORMATION

Corresponding Author

*E-mail: tiseanuc@yahoo.com, sutter@lcc-toulouse.fr, marius.andruh@dnt.ro.

■ ACKNOWLEDGMENT

Financial support from the CNCSIS (grant IDEI 506/2009) is gratefully acknowledged. We thank Professor V. I. Parvulescu and Dr. Delia Popescu (University of Bucharest, Faculty of Chemistry) for help with the X-ray powder diffraction measurements and Dr. S. Georgescu (National Institute for Laser, Plasma and Radiation Physics, Bucharest) for help with NIR emission measurements.

■ REFERENCES

(1) (a) Caravan, P.; Ellison, J. J.; McMurry, T. J.; Lauffer, R. B. *Chem. Rev.* **1999**, *99*, 2293. (b) Piguet, C.; Bunzli, J.-C. G. *Chem. Soc. Rev.* **1999**, *28*, 347. (c) Charbonniere, L.; Zeissel, R. F.; Guardigli, M.; Roda, A.; Sabbatini, N.; Cesario, M. *J. Am. Chem. Soc.* **2001**, *123*, 2436. (d) Parker, D. *Coord. Chem. Rev.* **2000**, *205*, 109. (e) Faulkner, S.; Pope, S. J. A.; Burton-Pye, B. P. *Appl. Spectrosc. Rev.* **2004**, *39*, 1. (f) Gunlaugsson, T.; Leonard, J. P. *Chem. Commun.* **2005**, 3114. (g) Leonard, J. P.; Gunnlaugsson, T. *J. Fluoresc.* **2005**, *15*, 585. (h) Pope, S. J. A.; Laye, R. H. *Dalton Trans.* **2006**, 3108.

(2) (a) Piguet, C.; Bunzli, J.-C. G.; Bernardinelli, G.; Hopfgartner, G.; Petoud, S.; Schaad, O. *J. Am. Chem. Soc.* **1996**, *118*, 6681. (b) Guerriero, P.; Tamburini, S.; Vigato, P. A. *Coord. Chem. Rev.* **1995**, *139*, 17. (c) Liu, W. S.; Jiao, T. Q.; Li, Y. Z.; Liu, Q. Z.; Tan, M. Y.; Wang, H.; Wang, L. F. *J. Am. Chem. Soc.* **2004**, *126*, 2280. (d) Hanaoka, K.; Kikuchi, K.; Kojima, H.; Urano, Y.; Nagano, T. *J. Am. Chem. Soc.* **2004**, *126*, 12470. (e) Sabbatini, N.; Guardogi, M.; Lehn, J. M. *Coord. Chem. Rev.* **1993**, *123*, 201. (f) Bunzli, J. G.; Piguet, C. *Chem. Soc. Rev.* **2005**, *34*, 1048. (g) Kido, J.; Okamoto, Y. *Chem. Rev.* **2002**, *102*, 2357. (h) Werts, M. H. V.; Woudenberg, R. H.; Emmerink, P. G.; van Gassel, R.; Hofstraat, J. W.; Verhoeven, J. W. *Angew. Chem., Int. Ed.* **2000**, *39*, 4542. (i) Hemmila, I. K. *Applications of Fluorescence in Immunoassays*; Wiley and Sons: New York, 1991. (j) Mathis, G. *Clin. Chem.* **1995**, *41*, 1391. (k) Faulkner, S.; Matthews, J. L. In *Comprehensive Coordination Chemistry, Applications of Coordination Complexes*, 2nd ed.; Elsevier: Amsterdam, 2003; Vol. 9. (l) Hemmila, I.; Laitala, V. *J. Fluoresc.* **2005**, *15*, 529. (m) Yuan, J.; Wang, G. *J. Fluoresc.* **2005**, *15*, 559. (n) Poupart, S.; Boudou, C.; Peixoto, P.; Massonneau, M.; Renard, P.-Y.; Romieu, A. *Org. Biomol. Chem.* **2006**, *4*, 4165. (o) De Silva, A. P.; Fox, D. B.; Huxley, A. J. M.; Moody, T. S. *Coord. Chem. Rev.* **2000**, *205*, 41. (p) Kolke, Y.; Okamoto, Y. *Chem. ReV.* **2002**, *102*, 2357. (q) Evans, R. C.; Douglas, P.; Winscom, C. J. *Coord. Chem. Rev.* **2006**, 2093. (r) Zhang, M.; Wang, J.; Zhang, Q.; Su, Q. *Appl. Phys. B: Lasers Opt.* **2007**, *86*, 647. (s) Sun, R. G.; Wang, Y. Z.; Zheng, Q. B.; Zhang, H. J.; Epstein, A. J. *J. Appl. Phys.* **2000**, *87*, 7589. (t) Sloof, L. H.; Polman, A.; Cacialli, F.; Friend, R. H.; Hebbink, G. A.; van Veggel, F. C. J. M.; Reinhoudt, D. N. *Appl. Phys. Lett.* **2001**, *79*, 3770. (u) Foley, T. J.; Harrison, B. S.; Knefely, A. S.; Abboud, K. A.; Reynolds, J. R.; Schanze, K. S.; Boncella, J. M. *Inorg. Chem.* **2003**, *42*, 5023. (v) De Bettencourt Dias, A. *Dalton Trans.* **2007**, 2229.

(3) (a) Sabbatini, N.; Guardigi, M.; Bolletta, F.; Manet, I.; Ziessel, R. *Angew. Chem., Int. Ed. Engl.* **1994**, *33*, 1501. (b) Yang, X.-P.; Jones, R. A. *J. Am. Chem. Soc.* **2005**, *127*, 7686.

(4) Sabbatini, N.; Guardigli, M.; Lehn, J.-M. *Coord. Chem. Rev.* **1993**, *123*, 201.

(5) (a) Whan, R. E.; Crosby, G. A. *J. Mol. Spectrosc.* **1962**, *8*, 315. (b) Bazzicalupi, C.; Bencini, A.; Bianchi, A.; Giorgi, C.; Fusi, V.; Masotti, A.; Valtancoli, B.; Roque, A.; Pina, F. *Chem. Commun.* **2000**, *7*, 561.

(6) (a) Kahn, O. *Molecular Magnetism*; Wiley-VCH: New York, 1993. (b) Benelli, C.; Gatteschi, D. *Chem. Rev.* **2002**, *102*, 2369.

(7) (a) Costes, J. P.; Novotchi, G.; Shova, S.; Dahan, F.; Donnadieu, B.; Laurent, J. P. *Inorg. Chem.* **2004**, *43*, 7792. (b) Novitchi, C.; Costes, J. P.; Donnadieu, B. *Eur. J. Inorg. Chem.* **2004**, 1808. (c) Costes, J. P.; Dahan, F.; Dupuis, A.; Laurent, J. P. *Inorg. Chem.* **1996**, *35*, 2400. (d) Koner, R.; Lee, G. H.; Wang, Y.; Wei, H. H.; Nohanta, S. *Eur. J. Inorg. Chem.* **2005**, 1500. (e) Mohanta, S.; Lin, H. H.; Lee, C. J.; Wei, H. H. *Inorg. Chem. Commun.* **2002**, *5*, 585. (f) Elmali, A.; Elerman, Y. *Z. Naturforsch.* **2003**, *58b*, 639. (g) Elmali, A.; Elerman, Y. *Z. Naturforsch* **2004**, *59b*, 535. (h) Elmali, A.; Elerman, Y. *Z. Naturforsch* **2004**, *59b*, 530. (i) Elmali, A.; Elerman, Y. *J. Mol. Struct.* **2005**, *737*, 29. (j) Costes, J. P.; Dahan, F.; Donnadieu, B.; Garcia-Tojal, J.; Laurent, J. P. *Eur. J. Inorg. Chem.* **2001**, 363. (j) Costes, J. P.; Clemente-Juan, J. M.; Dahan, F.; Dumestre, F.; Tuchagues, J. P. *Inorg. Chem.* **2002**, *41*, 2886. (k) Costes, J. P.; Dahan, F.; Wernsdorfer, W. *Inorg. Chem.* **2006**, *45*, 5. (l) Wong, W. K.; Liang, H.; Wong, W. Y.; Cai, Z.; Li, K. F.; Cheah, K. W. *New J. Chem.* **2002**, *26*, 275. (m) Yang, X. P.; Jones, R. A.; Wong, W. K.; Lynch, V.; Oye, M. M.; Holmes, A. L. *Chem. Commun.* **2006**, 1836. (n) Yang, X. P.; Jones, R. A.; Lynch, V.; Oye, M. M.; Holmes, A. L. *Dalton Trans.* **2005**, 849. (o) Yang, X. P.; Jones, R. A.; Wu, Q. Y.; Oye, M. M.; Lo, W. K.; Wong, W. K.; Holmes, A. L. *Polyhedron* **2006**, *25*, 271. (p) Lo, W. K.; Wong, W. K.; Guo, J. P.; Wong, W. Y.; Li, K. F.; Cheah, K. W. *Inorg. Chim. Acta* **2004**, *357*, 4510. (q) Wong, W. K.; Yang, X. P.; Jones, R. A.; Rivers, J. H.; Lynch, V.; Lo, W. K.; Xiao, D.; Oye, M. M.; Holmes, A. L. *Inorg. Chem.* **2006**, *45*, 4340. (r) Sakamoto, M.; Manseki, K.; Okawa, H. *Coord. Chem. Rev.* **2001**, *219−221*, 379. (s) Visinescu, D.; Madalan, A. M.; Andruh, M.; Duhayon, C.; Sutter, J.-P.; Ungur, L.; Van den Heuvel, W.; Chibotaru, L. F. *Chem.—Eur. J.* **2009**, *15*, 11808. (t) Sutter, J.-P.; Dhers, S.; Rajamani, R.; Ramasesha, S.; Costes, J.-P.; Duhayon, C.; Vendier, L. *Inorg. Chem.* **2009**, *48*, 5820. (u) Dhers, S.; Sahoo, S.; Costes, J.-P.; Duhayon, C.; Ramasesha, S.; Sutter, J.-P. *CrystEngComm.* **2009**, *11*, 2078.

(8) Hogerheide, M. P.; Boersma, J.; van Kotten, G. *Coord. Chem. Rev.* **1996**, *155*, 87.

(9) (a) Wong, W.-K.; Liang, H.; Wong, W.-Y.; Cai, Z.-W.; Li, K.-F.; Cheah, K.-W. *New J. Chem.* **2002**, *26*, 275. (b) Lo, W.-K.; Wong, W.-K.; Guo, J.-P.; Wang, W.-Y.; Li, K.-F.; Cheah, K.-W. *Inorg. Chim. Acta* **2004**, *357*, 4510. (c) Yang, X.-P.; Jones, R. A.; Lynch, V.; Oye, M. M.; Holmes, A. L. *Dalton Trans.* **2005**, 849. (d) Yang, X.-P.; Jones, R. A. *J. Am. Chem. Soc.* **2005**, *127*, 7686. (e) Wong, W.-K.; Yang, X.-P.; Jones, R. A.; Rivers, J. H.; Lynch, V.; Lo, W.-K.; Xiao, D.; Oye, M. M.; Holmes, A. L. *Inorg. Chem.* **2006**, *45*, 4340. (f) Yang, X.-P.; Jones, R. A.; Wu, Q.-Y.; Oye, M. M.; Lo, W.-K.; Wong, W.-K.; Holmes, A. L. *Polyhedron* **2006**, *25*, 271.

(g) Lo, W.-K.; Wong, W.-K.; Wong, W.-Y.; Guo, J.-P.; Yeung, K.-T.; Cheng, Y.-K.; Yang, X.-P.; Jones, R. A. *Inorg. Chem.* **2006**, *45*, 9315. (h) Yang, X.-P.; Jones, R. A.; Wong, W.-K.; Oye, M. M.; Holmes, A. L. *Chem. Commun.* **2006**, 1836.

(10) (a) Finger, L. W.; Cox, D. E.; Jephcoat, A. P. *J. Appl. Crystallogr.* **1994**, *27*, 892. (b) Larson, A. C., Von Dreele, R. B. *Los Alamos National Laboratory Report* **2004**, *86*, 748. (c) Thompson, P.; Cox, D. E.; Hastings, J. B. *J. Appl. Crystallogr.* **1987**, *20*, 79. (d) Toby, B. H. *J. Appl. Crystallogr.* **2001**, *34*, 210.

(11) (a) Andruh, M.; Costes, J.-P.; Diaz, C.; Gao, S. *Inorg. Chem.* **2009**, *48*, 3342. (b) Pasatoiu, T. D.; Madalan, A. M.; Kumke, M. U.; Tiseanu, C.; Andruh, M. *Inorg. Chem.* **2010**, *49*, 2310. (c) Tanase, S.; Andruh, M.; Müller, A.; Schmidtmann, M.; Mathonière, C.; Rombaut, G. *Chem. Commun.* **2001**, 1084. (d) Gheorghe, R.; Andruh, M.; Müller, A.; Schmidtmann, M. *Inorg. Chem.* **2002**, *41*, 5314. (e) Madalan, A. M.; Roesky, H. W.; Andruh, M.; Noltemeyer, M.; Stanica, N. *Chem. Commun.* **2002**, 1638. (f) Gheorghe, R.; Andruh, M.; Costes, J.-P.; Donnadieu, B. *Chem. Commun.* **2003**, 2778. (g) Gheorghe, R.; Cucos, P.; Andruh, M.; Costes, J.-P.; Donnadieu, B.; Shova, S. *Chem.—Eur. J.* **2006**, *12*, 187. (h) Andruh, M.; Branzea, D. G.; Gheorghe, R.; Madalan, A. M. *Cryst. Eng. Comm.* **2009**, *11*, 2571. (i) Branzea, D. G.; Sorace, L.; Maxim, C.; Andruh, M.; Caneschi, A. *Inorg. Chem.* **2008**, *47*, 6590. (j) Branzea, D. G.; Guerri, A.; Fabelo, O.; Ruiz-Pérez, C.; Chamoreau, L.-M.; Sangregorio, C.; Caneschi, A.; Andruh, M. *Cryst. Growth Des.* **2008**, *8*, 941.

(12) Brito, H. F.; Malta, O. L.; Felinto, M. C. F. C.; Teotonio, E. E. S.; Menezes, J. F. S.; Silva, C. F. B.; Tomiyama, C. S.; Carvalho, C. A. A. *J. Alloys Compd.* **2002**, *344*, 293.

(13) Sun, W.-B.; Yan, P.-F.; Li, G.-M.; Xu, H.; Zhang, J.-W. *J. Sol. State Chem.* **2009**, *182*, 381.

(14) Gonalves e Silva, F. R.; Malta, O. L.; Reinhard, C.; Gudel, H.-U.; Piguet, C.; Moser, J. E.; Bunzli, J.-C. G. *J. Phys. Chem. A* **2002**, *106*, 1670.

(15) Stein, G.; Wurzberg, E. *J. Chem. Phys.* **1975**, *62*, 208.

(16) (a) Brunet, E.; Alonso, M.; Juanes, O.; Velasco, O.; Rodrguez-Ubis, J. *Tetrahedron* **2001**, *57*, 3105. (b) Howell, R. C.; Spence, K. V. N.; Kahwa, I. A.; White, A. J. P.; Williams, D. J. *J. Chem. Soc., Dalton Trans.* **1996**, 961. (c) Guerriero, P. A.; Vigato, P. A.; Bunzli, J.-C. G.; Moret, E. *J. Chem. Soc., Dalton Trans.* **1990**, 647. (d) Rodríguez-Cortiñas, R.,; Avecilia, F.; Platas-Iglesias, C.; Imbert, D.; Bünzli, J.-C. G.; De Blas, A.; Rodríguez-Blas, T. *Inorg. Chem.* **2002**, *41*, 5336.

(17) Feng, W.; Hui, Y.; Wei, T.; Lu, X.; Song, J.; Chen, Z.; Zhao, S.; Wong, W. K.; Jones, R. A *Inorg. Chem. Commun.* **2011**, *14*, 75 (Nd anion).

(18) Comby, S.; Bünzli, J.-C. G. In *Handbook on the Physics, Chemistry of Rare Earths*; Gschneidner, K. A., Jr., Bünzli, J.-C. G., Pecharsky, V. K., Eds.; Elsevier Science B.V.: Amsterdam, 2007; Vol. 37, Chapter 235, p 217.

(19) Andruh, M.; Bakalbassis, E.; Kahn, O.; Trombe, J. C.; Porcher, P. *Inorg. Chem.* **1993**, *32*, 1616.

(20) (a) Sutter, J.-P.; Kahn, M. L. In *Magnetism: molecules to materials Vol. 5*;Miller, J. S., Drillon, M., Eds.; Wiley-VCH: New York, 2005; p 161. (b) Sutter, J.-P.; Kahn, M. L.; Kahn, O. *Adv. Mater.* **1999**, *11*, 863. (c) Kahn, M. L.; Sutter, J.-P.; Golhen, S.; Guionneau, P.; Ouahab, L.; Kahn, O.; Chasseau, D. *J. Am. Chem. Soc.* **2000**, *122*, 3413. (d) Sutter, J.-P.; Kahn, M. L.; Mörtl, K. P.; Ballou, R.; Porcher, P. *Polyhedron* **2001**, 1593. (e) Kahn, M. L.; Ballou, R.; Porcher, P.; Kahn, O.; Sutter, J.-P. *Chem.—Eur. J.* **2002**, *8*, 525.